TEMPORAL RESOLUTION IMPROVEMENT IN DYNAMIC SPECKLE ANALYSIS

Mikhail Levchenko*, Elena Stoykova, Violeta Madjarova

Institute of Optical Materials and Technologies, Bulgarian Academy of Sciences, Acad. Georgi Bonchev, Bl.109, 1113 Sofia, Bulgaria

Abstract

Dynamic speckle imaging is effective approach for visualization of areas of faster or slower micro-changes on a 3D object surface by analysis of speckle patterns formed on this surface under laser illumination. A 2D distribution of a statistical parameter related to the measured speed of changes is built as a map of activity. The map entries strongly fluctuate from point to point even when the speed is constant in the observed area. The relevant information is buried in a signal-dependent noise, which depends on (1) activity, and (2) ratio between the time of acquisition of the speckle patterns in the sequence and the temporal correlation radius of the process. The time of acquisition gives the temporal resolution of the method. In order to improve this resolution, we studied acquisition at time interval between the patterns that is much shorter than the temporal correlation radius of intensity fluctuations caused by the underlying processes in the tested object.

Keywords: *dynamic speckle, temporal resolution, simulation, optimization*

1. INTRODUCTION

Dynamic speckle imaging (DSI) has found applications in different areas for monitoring capillary blood flow [1], non-destructive analysis of ceramics [2], bacterial response [3] and paint drying [4] to name a few. This technique is based on the interference phenomenon [5, 6]. A laser speckle pattern is randomly produced by addition of surface-scattered coherent light under laser illumination of the tested object. To capture a speckle pattern, a CCD or CMOS camera is used. Due to processes ongoing within the object, speckle pattern changes in time. To estimate the speed of these changes, algorithms, based on capturing sets of images, correlated in time, were proposed. Among them, pointwise processing algorithms are one of the most developed and commonly used methods for analysis of multiple speckle patterns. They allow to build activity distribution maps, further named activity maps [7] by processing intensities at each pixel with the same coordinates in the set of the acquired speckle images. Intensity values strongly fluctuate within the recorded patterns, and hence one observes fluctuations in the activity maps even if activity within the sample doesn't change. This results in decreasing contrast of the activity maps and thus impairs sensitivity and spatial resolution of the pointwise processing algorithms. In order to decrease the spread of fluctuations in the maps, the time for capturing a set of speckle images, used to calculate a given activity map, should be increased. Temporal resolution, in its turn, depends on time for data acquisition of the single set and is given by $T = N \times \Delta t$, where N is the number of correlated in time speckle images and Δt is the time interval between two successive images. Thus, increasing the number of the speckle images N decreases temporal resolution of the DSI method. Choice of the time interval Δt is task specific and is related to the temporal correlation radius τ_c of the intensity fluctuations caused by the process under monitoring. Thus, choice of the optimal acquisition time, T, of speckle images in order to provide reasonable temporal resolution and good quality of the activity map is one of the most important tasks in the measurement.

This paper is dedicated to the task of improving DSI temporal resolution. This is crucial for conducting experiments with samples and fluids, which exhibit relatively fast changes. In order to study the influence of temporal resolution, T, on the quality of the built maps, we carried out a set of synthetic experiments.

First, we have studied how acquisition at time interval between the successive images, that is much shorter than temporal correlation radius of intensity fluctuations, affects quality of the obtained activity maps. As a second step, we have examined the impact of time resolution, including number of analyzed speckle images, on the contrast of built activity maps. As a metric for evaluation of activity map quality, a probability density function (PDF) has been used. Finally, we have carried out a set of experiments in order to check correctness of our statements, based on simulated data.

2. TIME RESOLUTION ANALYSIS - SIMULATION

2.1. Pointwise intensity-based measurement, algorithms and simulation approach

2.1.1. Experiment setup

The experimental setup for capturing speckle patterns is shown in Fig.1. An object under study is placed on the vibration isolated table. An expanded laser beam with wavelength λ = 632.8 nm illuminates the sample. Normally to the object surface, a camera captures scattered coherent light with phase and intensity changes in time due to activity in the sample. Resolution of the captured images is $N_x \times N_y$ pixels and a pixel interval is Δ.

The basics of the pointwise processing is explained in Fig. 2 [8]. To build a single activity map, a set of N correlated in time speckle images is used, and, thus, time resolution is given by $T = N \text{ x } \Delta t$. For the map, an estimate is calculated for every set $I_{p,n} = [I_{p,1}, I_{p,2}, \ldots, I_{p,N}]$, where p is a pixel in the range (1... N_x)(1…N_y) and n is the current number of the speckle image in the set. The images are temporally correlated in time due to a proper choice of time interval Δt. A parameter, that describes temporal intensity correlation in data sets and is related to activity is temporal correlation radius $\tau_c(x,y)$ [8]. The larger correlation radius, the lower activity.

Commonly used algorithms applied in building activity maps are calculation of the generalized differences (GD) [9, 10], the weighted generalized differences (WGD) [11], Fujii algorithm [12, 13], the structure function (SF) and the modified structure function (MSF) [14]. The MSF algorithm, which provides good quality of the map, is the simplest. It is based only on one summation, hence it works faster compared to GD and WGD algorithms. In this study, activity maps were built using non-normalized and normalized MSF algorithms. The normalized one is used in order to overcome issues with spatially variable speckle statistics, related to slight non-uniformity of illumination. All simulations were conducted at uniform illumination and therefor the non-normalized MSF algorithm was used:

$$S(p,m) = \frac{1}{N-m} \sum_{i=1}^{N-m} \left| I_{p,i} - I_{p,i+m} \right|, \tag{1}$$

where m is an integer and time-lag $\tau = m\Delta t$ shows the difference in time between the compared speckle images in the set. If $\tau > \tau_c$, then correlation of intensities between the analyzed speckle images is low.

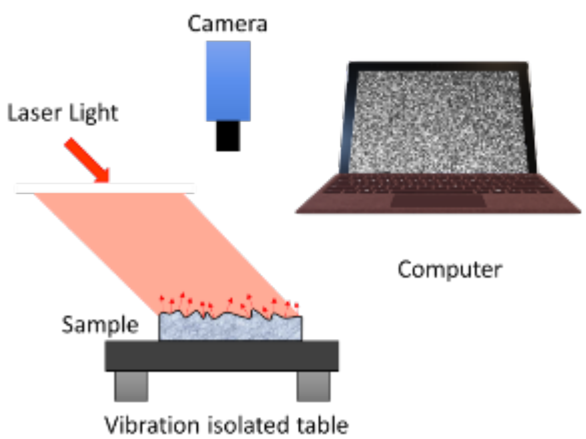

Fig. 1. Experimental setup for capturing speckle pattern images

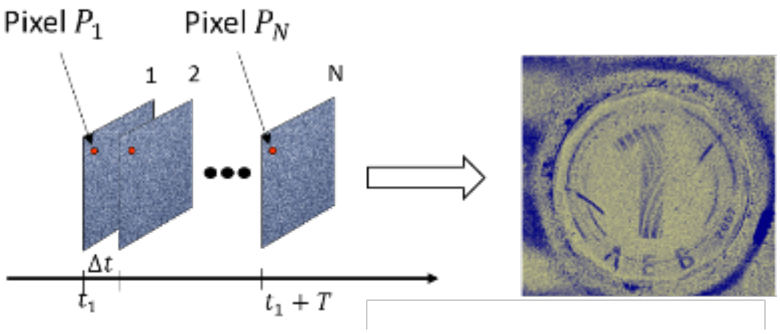

Fig. 2. Building MSF activity map from a set of *N* time-correlated speckle images; the object is a coin of 1 Lev covered with a non-transparent paint.

2.1.2. Quality of activity map as a function of Δt and N

To evaluate the impact of the time interval Δt between successively captured images on quality of activity maps, we carried out numerical experiments with simulated speckle images of a specially designed test object shown in Fig. 3. The simulation included the following steps:

1) generation of 2D set of random delta-correlated in space phase values uniformly distributed in range (0…2π);
2) generation of a 2D set of correlation radius $\tau_c(\frac{x\Delta}{2}, \frac{y\Delta}{2})$, $x = 1 \dots N_x$; $y = 1 \dots N_y$, in order to simulate regions with different activity values;
3) generation of 2D set of correlated in time wrapped phase distributions which are delta-correlated in space; for temporal correlation normalized auto-correlation function $\rho_{xy}(\tau) = \exp[-\tau/\tau_c(\frac{x\Delta}{2}, \frac{y\Delta}{2})]$ has been applied [15];
4) simulation of the complex amplitude U_s of the light reflected from the observed object. $U_s = \sqrt{I_0}\exp[-j\varphi(\frac{x\Delta}{2}, \frac{y\Delta}{2}, i\Delta t)]$ where I_0, is the intensity of the laser beam;
5) simulation of the complex amplitude of light falling on the CCD matrix as $U_{CCD} = FT^{-1}[H \cdot FT(U_s)]$, where *H* is the coherent transfer function of the registration system and FT is Fourier Transform;
6) simulation of integration of intensity distribution by a CCD camera matrix with pixel size Δ.

The simulated object consists of 4 rectangular areas A1, A2, A3, A4 with different constant activities given by $\tau_{c1}, \tau_{c2}, \tau_{c3}$ and τ_{c4}. Activity maps are built by applying the MSF algorithm to 256 simulated speckle images, hence acquisition time is $T = 256\Delta t$. The size of each rectangular region is 64 x 256 pixels, which allows to build rather accurately a histogram of the MSF estimate as an estimate of its PDF which is an effective quality metric for the obtained activity maps.

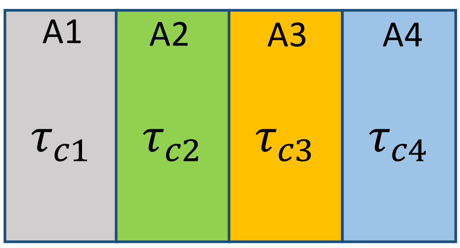

Fig. 3. Simulated test object with four rectangular regions with different temporal correlation radii

The first simulation corresponds to the case when the temporal radius of correlation of the observed process is unknown. We choose some Δt and the time lag in Eq.(1) equal to $\tau = 10\Delta t$. We modeled three hypothetic situations. In the first case, Δt is equal to τ_c of the fastest process, and the values of the correlation radii are as follows: $\tau_{c1} = \Delta t; \tau_{c2} = 2\Delta t; \tau_{c3} = 3\Delta t; \tau_{c4} = 4\Delta t$. In the second numerical experiment, Δt is less than τ_c of the fastest process, i.e. $\tau_{c1} = 10\Delta t; \tau_{c2} = 20\Delta t; \tau_{c3} = 30\Delta t; \tau_{c4} = 40\Delta t$. Finally, in the last case, Δt is much smaller than τ_c and the values are: $\tau_{c1} = 100\Delta t; \tau_{c2} = 200\Delta t; \tau_{c3} = 300\Delta t; \tau_{c4} = 400\Delta t$. Below in Figs. 4 (a, c, e), the activity maps for the three simulations are shown respectively. Figures 4 (b, d, f) present the histograms of the MSF estimate for the four areas in the built activity maps.

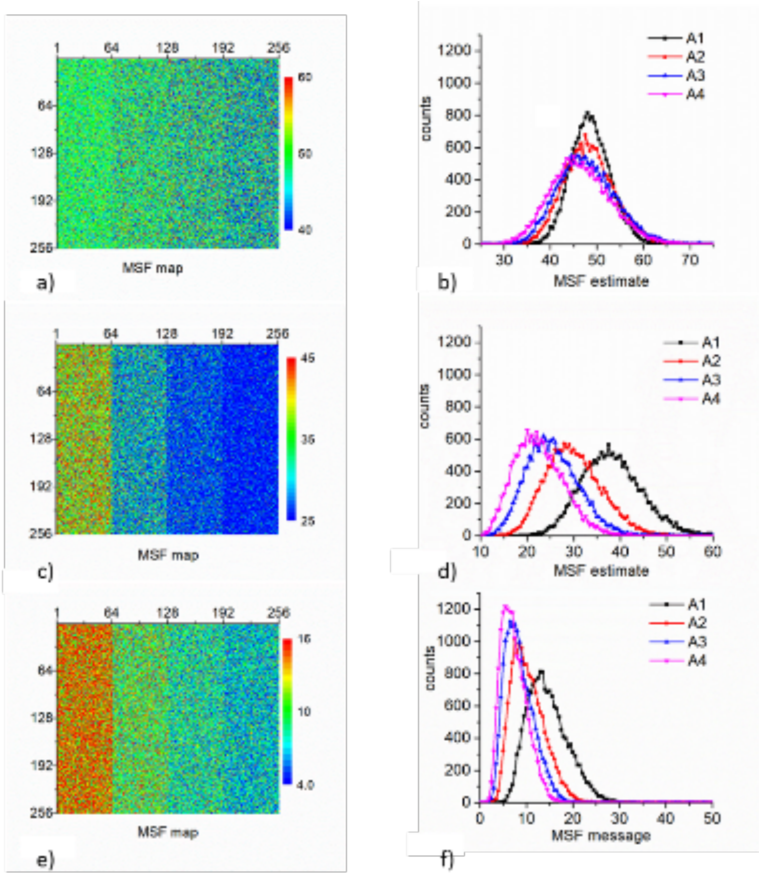

Fig. 4. Built activity maps (left) and their respective histograms of MSF estimate (right): a), b) - Δt is equal to τ_{c1}; c), d) - Δt is less than τ_{c1}; e), f) - Δt is much less than τ_c

When Δt is equal to τ_{c1}, the activity areas characterized by $\tau_{c1}, \tau_{c2}, \tau_{c3}$ and τ_{c4} are barely recognizible. The ratio T/τ_{ci} , i = 1,2,3,4 is large, being equal in the four cases to 256, 128, 85 and 64 respectively. This and the too larger time lag τ lead to weak temporal correlation of the data and hence to poor sensitivity of the method. The spread of the histograms is large, and they overlap each other which results in low contrast of the activity map. In the second simulation, the ratio T/τ_{ci} , i = 1,2,3,4 is still rather large being equal in the four cases to 25.6, 12.8, 8.5, and 6.4 The time lag is equal to the radius of correlation of the fastest process. This case corresponds to well correlated data on one side and to rather long realizations of the fluctuating intensity. Regions of different activity can be easily distinguished. The spread of histograms is also large, but they overlap to much lesser extent. In the third simulation, the ratio T/τ_{ci} , i = 1,2,3,4 is rather small, being equal in the four cases to 2.56, 1.28, 0.85, and 0.64. The time lag is much less than the radius of correlation of the fastest process. This corresponds to very correlated data and thus to rather short realizations of the fluctuating intensity. The activity map shows better contrast than in Fig. 4 a), but worse than in Fig. 4 c). The histograms are narrower, but they ovelap significantly. Although the activity map with the best contrast is obtained in the second simulation, the third one provides very encouraging results: it is possible significantly to decrease Δt with respect to the temporal correlation radius of intensity fluctuations and to detect different activities at $N = 256$ images.

In the next simulation, we have explored time resolution impact on quality of the activity map. For this purpose, 1024 speckle pattern images for the object in Fig. 3 were generated at interval δ between two successive images, that was chosen rather small compared to the correlation radii of the observed processes. Activity values of the simulated sample were : $\tau_{c1} = 40\delta; \tau_{c2} = 80\delta; \tau_{c3} = 160\delta; \tau_{c4} = 320\delta$. Using these patterns, three synthetic experiments have been carried out with $N = 256$ at $\Delta t = \alpha\delta$ for α being an integer equal to 1, 2 and 4 to build activity maps and histograms corresponding to decreasing acquisition time. Accordingly, the time lag was taken equal to $\tau = \alpha \times 10\Delta t$ to provide MSF estimate values within the same interval in the three cases. In the first simulation, $\alpha = 4$ and temproral resolution is determined as $T_1 = 4N\delta$. Temporal correlation radius values in units of Δt are: $\tau_{c1} = 10\Delta t; \tau_{c2} = 20\Delta t; \tau_{c3} = 40\Delta t; \tau_{c4} = 80\Delta t$. On the next step, $\alpha = 2$, activity values are: $\tau_{c1} = 20\Delta t; \tau_{c2} = 40\Delta t; \tau_{c3} = 80\Delta t; \tau_{c4} = 160\Delta t$. For the last simulation $\alpha = 1$, temporal resolution is $T = T_1/4$ and temporal correlation radius values are: $\tau_{c1} = 40\Delta t; \tau_{c2} = 80\Delta t; \tau_{c3} = 160\Delta t; \tau_{c4} = 320\Delta t$. As in the first sythetic experiment, PDF is used to evaluate contrast and sensitivity of the obtained activity maps. In Figs. 5 (a, c, e), activity maps are shown for the three values of α. As well, PDFs of the estimates for these activity maps are shown in Figs. 5 (b, d, f).

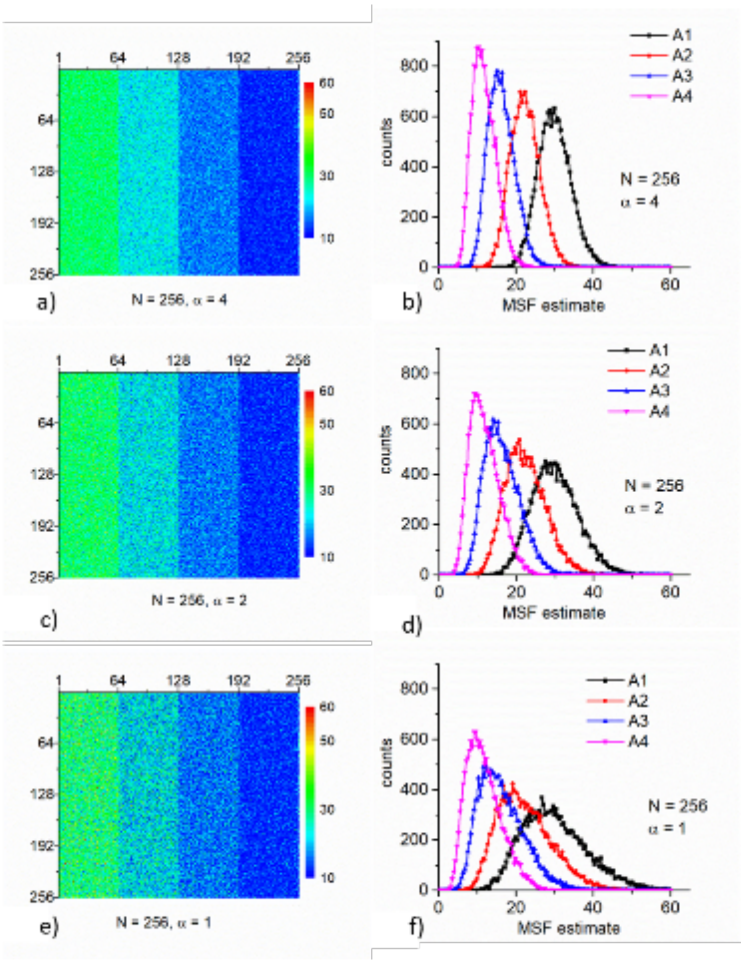

Fig. 5. Built activity maps (left) and the respective histograms of the MSF estimate (right): a), b) - $\alpha = 4$; temporal resolution: $T = T_1$; c), d) $\alpha = 2$, temporal resolution $T = \frac{T_1}{2}$;e), f) $\alpha = 1$, temporal resolution $T = \frac{T_1}{4}$.

One may notice that the contrast of all images makes it easy to distinguish between different areas of activity. In addition, as it was expected, with time resolution increasing or time T decreasing, fluctuations of the estimates also increase. This is easily proven by the histograms. In the first numerical experiment with activity regions $\tau_{c1} = 10\Delta t; \tau_{c2} = 20\Delta t$; $\tau_{c3} = 40\Delta t$; $\tau_{c4} = 80\Delta t$, histograms are narrow and slightly overlap each other. With improvement of the temporal resolution, spread of histograms is expanding, fluctuations are increasing and contrast worsens. Nevertheless, the obtained activity map with temporal resolution $T = T_1/4$ still shows satisfactory result. The MSF map entries fluctuate, but the different activity regions are still distinguishable.

The good results obtained for the case of temporal resolution $T = T_1/4$ motivated us to apply filtering to the activity maps as it has been described in [16]. The MSF activity maps for 256 and 128 speckle images are shown in Fig. 6 (a) and Fig. 6 (c). After maps filtering, in both tests, spread of fluctuations has become much narrower and the histograms almost do not overlap each other (Fig.6). Thus, one can make a conclusion that it is possible to obtain satisfactory activity maps using small interval Δt and only 128 speckle images and, hence, to improve 8 times temporal resolution.

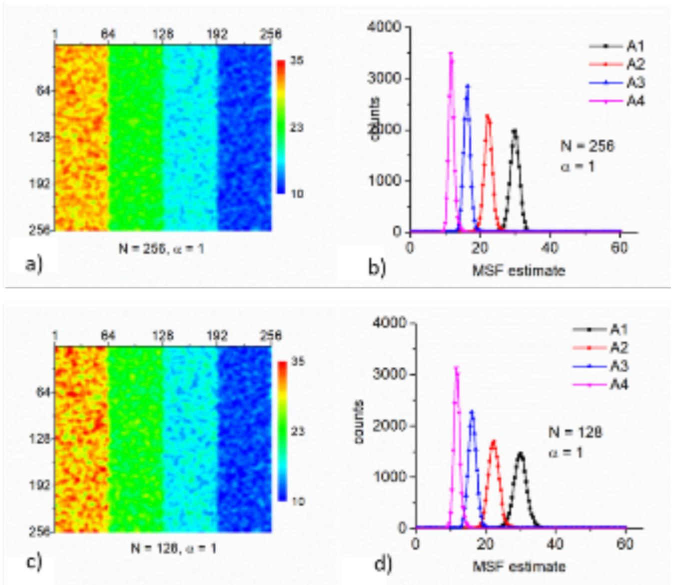

Fig. 6. Filtered activity maps and histograms, built by analyzing: (a) 256 speckle images, (c) 128 speckle images histograms

3. DRYING POLYMER EXPERIMENT

An experiment with a drying polymer was carried out in order to confirm results, obtained by simulations. Raw data were acquired for thin polymer films. The latter are required for a variety of applications with stringent requirements set on homogeneity, thickness uniformity, surface smoothness, transparency and optical quality. Spatial characterization of speed of evaporation for a deposited layer of a polymer solution allows for controlling its quality. In this study, we used commercially available from Sigma Aldrich azopolymer poly [1-[4-(3-carboxy-4-hydroxy-phenylazo) benzene-sulfonamido]-1,2-ethanediyl, sodium salt] or PAZO. It is soluble in water and methanol. For the experiment, 40 mg of azopolymer PAZO were dissolved in 400 µL of a suspension of water. A 100 µl droplet was spread on a glass substrate. The speckle pattern formed on the glass is shown in Fig. 7 as a bitmap image and a 3D map. Spatially variable speckle statistics, obviously related to slight non-uniformity of illumination, characterizes the shown pattern. For this experiment normalized MSF algorithm was used in order to overcome this drawback:

$$S(p,m) = \frac{1}{N-m} \sum_{n=1}^{N-m} \left| I_{p,n} - I_{p,n+m} \right| / \left(I_{p,n} + I_{p,n+m} \right) \quad (2)$$

Several sets of 256 correlated in time speckle patterns were recorded at the time offsets $t = 0$, 2, 4 and 6, min from the start of the experiment. The optical set-up was positioned on an optical table with active vibro-isolation. The activity maps computed at $\tau = 10\Delta t_{1,2}$ from 8-bit encoded patterns are shown in Fig. 8 for $N = 64$. The upper row in Fig. 8 corresponds to $\Delta t_2 = 4\Delta t_1$; lower row: $\Delta t_1 = 250$ ms.

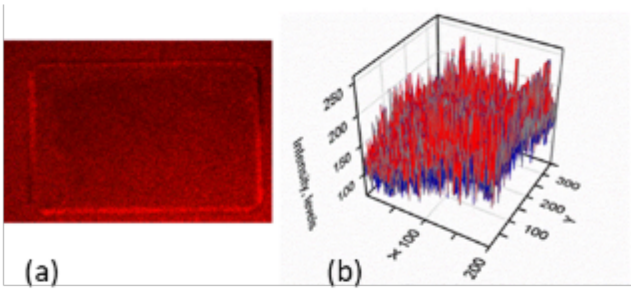

Fig. 7. (a) Bitmap speckle image and (b) 3D distribution of the intensity

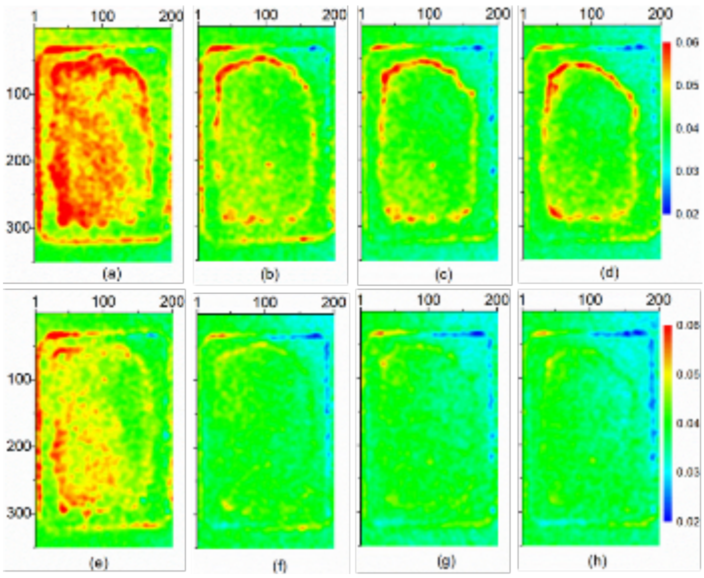

Fig. 8. Activity maps from left to right, recorded at the time offsets t = 0, 2, 4 and 6, min from the start of the experiment. Upper row - $\Delta t_2 = 1$ s. Lower row - $\Delta t_1 = 250$ ms.

The activity maps in Fig.8 are obtained with time resolution 64 s and 16 s from sets of images acquired at different time offsets. The maps correspond to time lags 10 s and 2.5 s respectively. At the chosen time lags, the MSF estimate given by Eq. (2) varies practically within the same interval of values for both resolutions. Process of polymer drying is observable at every time offset for both time resolutions. Regions with faster drying polymer are easily observed at initial time offset t = 0 min. Activity changing is especially evident on the edges of PAZO spread. The obtained activity maps show better contrast with the time resolution $T_2 = N \times \Delta t_2 = 64$ s. Despite the less contrast of the maps corresponding to 16 s time of acquisition, these maps properly reflect decrease of activity in the sets of images at time offsets t = 2 min, 4 min and 6 min.

Thus, theoretical results, obtained in series of simulations have been experimentally proven. We see that increasing time resolution inevitably worsens the quality of the activity maps, but the latter is still satisfactory for performing DSI.

4. DISCUSSION

In summary, we have analyzed options for temporal resolution improvement in the pointwise dynamic speckle imaging. We have carried out set of simulations and an experiment in order to study influence of acquisition time, *T*, which gives the temporal resolution, on quality of activity maps. The latter visualize as an instant picture the areas of faster or slower developing processes on the surface of the tested object.

In the first set of simulations, we have analyzed the choice of the time interval between the successive images, Δt, with respect to the temporal correlation radius τ_c of the observed process. We found out that $\Delta t \sim \tau_c$ worsens the MSF map contrast. The spread of the PDF of the MSF estimate is large, and the PDFs overlap each other at different activities. Best quality was obtained in the case when Δt is a few times less than τ_c. Regions of different activity within a synthesized object can be easily distinguished. The spread of PDFs is also large, but they overlap to much lesser extent. When Δt is 100 times less than τ_c, the PDFs are narrower, but they ovelap significantly, which leads to map contrast decreasing. Nevertheless, visualization of regions of different activity is possible which directly means that improvement of the temporal resolution by choosing $\Delta t \ll \tau_c$ is feasible.

In the second set of simulations, the assumption that fluctuations within a MSF map corresponding to the same mean activity increase in their spread at decreasing T was confirmed. Nevertheless, in case when time resolution of the method is 4 times better, quality is still acceptable.

Going further, we have done simulation with decreasing number *N* of the analyzed speckle images. Quality of activity maps with reduced number *N* remained satisfactory.

Finally, we have carried out set of experiments with azopolymer that demonstrate that increasing of the temporal resolution decreases contrast of activity maps. However, contrast does not worsen critically.

ACKNOWLEDGMENTS

M. Levchenko thanks 2020 Plenoptic Imaging project for supporting his PhD training. This project has received funding from the European Union's Horizon 2020 research and innovation programme under the Marie Skłodowska-Curie grant agreement No 956770. E. Stoykova thanks European Regional Development Fund within the Operational Programme "Science and Education for Smart Growth 2014–2020" under the Project CoE "National centre of Mechatronics and Clean Technologies" BG05M2OP001-1.001-0008. The authors would like to thank L. Nedelchev and B. Blagoeva for their help in conducting experiments with polymer drying.

REFERENCES

1. M.Z. Ansari, A.K. Nirala, 2015, "Monitoring capillary blood flow using laser speckle contrast analysis with spatial and temporal statistics", *Optik*, vol. 126, no. 24, 2015, pp. 5224-5229.
2. Chen, L., Cikalova, U., Bendjus, B., Muench, S., and Roellig, M., 2020, "Characterization of ceramics based on laser speckle photometry", *J. Sens. Sens. Syst*., 9, pp, 345–354.
3. Zhou K, Zhou C, Sapre A, Pavlock JH, Weaver A, Muralidharan R, Noble J, Chung T, Kovac J, Liu Z, Ebrahimi A., 2020, "Dynamic Laser Speckle Imaging Meets Machine Learning to Enable Rapid Antibacterial Susceptibility Testing (DyRAST)", *ACS Sens*, vol.5, no.10, pp. 3140-3149.
4. Faccia, P.A., 2009, "Differentiation of the drying time of paints by dynamic speckle interferometry". *Progress in Organic Coatings*, vol.64, no. 4, pp. 350–355.

5. J. W. Goodman, 1976, "Some fundamental properties of speckle," *J. Opt. Soc. Am*, 66, pp. 1145.
6. J. W. Goodman, 1984, "Laser Speckle and Related Phenomena", *Springer Verlag*
7. Stoykova E, Nazarova D, Berberova N, Gotchev A., 2015, "Performance of intensity-based non-normalized pointwise algorithms in dynamic speckle analysis", *Opt Express*., vol. 23, no. 19, pp. 25128-42.
8. Elena Stoykova, Blaga Blagoeva, Natalya Berberova-Buhova, Mikhail Levchenko, Dimana Nazarova, Lian Nedelchev, and Joongki Park, 2022, "Intensity-based dynamic speckle method using JPEG and JPEG2000 compression", *Appl. Opt.,* 61, B287-B296
9. R. Arizaga, N. Cap, H. Rabal, and M. Trivi, 2002, "Display of the local activity using dynamical speckle patterns," *Optical Engineering*, vol. 41, p. 287.
10. G. Romero, E. Alans, and H. Rabal, 2000, "Statistics of the dynamic speckle produced by a rotating diffuser and its application to the assessment of paint drying," *Optical Engineering*, vol. 39, no. 6, p. 1652.
11. H. J. Rabal, 2008, "Dynamic Laser Speckle and Applications", *CRC Press*, pp. 115–136.
12. H. Fujii, T. Asakura, K. Nohira, Y. Shintomi, and T. Ohura, 1985, "Blood flow observed by time-varying laser speckle", *Opt. Lett.*, 10, pp. 104–106.
13. H. Fujii, K. Nohira, Y. Yamamoto, H. Ikawa, and T. Ohura, 1987, "Evaluation of blood flow by laser speckle image sensing. Part 1", *Appl. Opt.,* 26, pp. 5321–5325.
14. E. Stoykova, B. Ivanov, and T. Nikova, 2014, "Correlation-based pointwise processing of dynamic speckle patterns", *Opt. Letters,* vol. 39, no. 1, pp.115–118.
15. A. Federico, G. Kaufmann, G. Galizzi, H. Rabal, M. Trivi, and R. Arizaga. 2006, "Simulation of dynamic speckle sequences and its application to the analysis of transient processes", *Optics Communications*, vol. 260, no. 2, pp. 493-499.
16. Elena Stoykova, Natalia Berberova, Youngmin Kim, Dimana Nazarova, Branimir Ivanov, Atanas Gotchev, Jisoo Hong, and Hoonjong Kang, 2017, "Dynamic speckle analysis with smoothed intensity-based activity maps", *Optics and Lasers in Engineering*, vol.93.